Electron localization in disordered graphene for nanoscale lattice sizes: multifractal properties of the wavefunctions

2014 2D Mater. 1 011009

(http://iopscience.iop.org/2053-1583/1/1/011009)

2D Materials

Letter

Electron localization in disordered graphene for nanoscale lattice sizes: multifractal properties of the wavefunctions

J E Barrios-Vargas[1] **and Gerardo G Naumis**[1]

[1] Depto. de Física-Química, Instituto de Física, Universidad Nacional Autónoma de México (UNAM) Apdo. Postal 20-364, 01000, México DF, México
E-mail: jebarrios@fisica.unam.mx and naumis@fisica.unam.mx

Received 27 November 2013, revised 12 March 2014
Accepted for publication 8 April 2014
Published 29 May 2014

2D Materials **1** (2014) 011009

doi:10.1088/2053-1583/1/1/011009

Abstract

An analysis of the electron localization properties in doped graphene is performed by carrying out a numerical multifractal analysis for finite systems of a size smaller than the possible localization length. By obtaining the singularity spectrum of a tight-binding model, it is found that the electron wave functions present a multifractal behavior for systems up to 20 nm. Such multifractality is preserved even for next-to-nearest neighbor hopping interaction, which needs to be taken into account if a comparison with experimental results is desired. States close to the Dirac point have a wider multifractal character than those far from this point as the impurity concentration is increased. The analysis of the results allows one to conclude that in the split-band limit, where impurities act as vacancies, the system can be described well by a chiral orthogonal symmetry class.

Keywords: graphene, electron mobility, localized states

Ever since its discovery [1, 2], graphene has been considered an ideal candidate to replace silicon in electronics [3], since this first truly two-dimensional crystal has the highest known electrical and thermal conductivity [4]. However, graphene *per se* is not a semiconductor. Several proposals have been made to solve this issue [5]. Experimentally, it has been found that doped graphene presents a metal-to-insulator transition [6] when doped with H, producing a kind of narrow band gap semiconductor. The increase in localization around the Dirac point was roughly predicted from an electron wavefunction frustration analysis in the graphene's underlying triangular lattice [7–9]. Such theoretical results were made under the supposition

that hydrogen bonds to the $2p_z$ carbon orbital, and thus impurities act as vacancies [10, 11]. This case corresponds to the split-band limit. This approach has been useful for predicting a pseudo localization transition and the pseudogap size, i.e., the region in which the inverse participation ratio increases by one order of magnitude [7] in very good agreement with experiments [6], although vacancies and impurities are indeed different [12–14]. However, there is a theoretical nuance to the idea of having a metal-insulator transition in two dimensions (2D). According to the well known Abraham *et al* scaling analysis, in 1D and 2D all states are localized for any amount of disorder, excluding the possibility of a mobility edge [15]. In spite of this, for 2D the situation is not completly clear yet since the community seems to be split into two groups [16], one denies the existence of non-exponential localized states [17, 18], while the other reports such states [16, 19, 20]. For example, a highly efficient expansion technique coupled with a huge finite-size scaling analysis showed non-localized states [16] with a multifractal behavior [21] in a square lattice with sustitutional disorder, akin to the one considered in this letter. Such theoretical debate has heated-up by the discovery of graphene, since some experimental and numerical results show that not all states are localized [6, 22–24], and there exists a kind of mobility edge associated with a pseudogap around the Fermi energy [7, 9, 25–27]. Other groups claim that all states are localized for disorder with intervalley mixing [28].

Thus, there is a debate that has not yet been settled. It is worth mentioning here that part of the problem is that general conclusions are made without taking care of the different kinds of disorder. For example, the Anderson type of disorder is not the same as the binary sustitutional one. However, there are three possibilities concerning delocalization in graphene: (i) either electron–electron interaction produces delocalization [29], (ii) the analysis by Abraham *et al* does not completely apply to some cases or (iii) the computations made are always smaller than the localization length of some states. In graphene, electron–electron interaction is very weak [30], so in principle, the first option can be ruled out, leaving (ii) and (iii) as the source of the discrepancies. This subject has been explored partially in previous publications, where critical states, i.e. states decaying as a power law, have been observed in finite lattices [26, 31, 32]. In addition, such a possibility has been considered in previous studies concerning quantum percolation in 2D [33–35], since the model presented in this letter is in the limit of very different self-energy impurities reduces the problem to site percolation (see below).

Notice that the scenario posed by (iii) does not rule out the observation of critical states for lattices with a size smaller than the localization length. As is well known, in this situation the exponent spectrum looks multifractal [29]. For graphene, this can be predicted by a symmetry breaking analysis [29], since the extra symmetries of the graphene's lattice makes the problem different from a generic 2D Fermi gas [26]. The idea behind this is to make a random matrix analysis of broken symmetries in the Dirac Hamiltonian when disorder is introduced [29]. In this analysis, a classification of the symmetries leads to different universality classes in the transition. Although all these points have been around for a while, few numerical results are available that analyze such questions [36, 37]. Here we provide such an analysis, showing that multifractal states are present in doped graphene for finite systems, in which the size is smaller than the possible localization length. Our results imply that the conductance of doped graphene will have an anomalous dependence upon the system length and applied electric field. In particular, experiments in graphene doped with adatoms from group I are ideal for measuring such effects [6].

Let us consider doped graphene as a honeycomb lattice with substitutional impurities placed at random with a uniform distribution. The corresponding π orbital one electron tight-binding Hamiltonian is [38],

$$\mathcal{H} = -t\sum_{\langle i,j\rangle}\left|\boldsymbol{i}\right\rangle\left\langle\boldsymbol{j}\right| - t'\sum_{\langle\langle i,j\rangle\rangle}\left|\boldsymbol{i}\right\rangle\left\langle\boldsymbol{j}\right| + \varepsilon\sum_{\ell}\left|\ell\right\rangle\left\langle\ell\right|. \tag{1}$$

The first sum is over nearest neighbors, with $t = 2.79$ eV the hopping energy [39]. The second sum is carried over next-to-nearest neighbors. Here we will consider two cases, $t' = 0$ eV which is the most studied Hamiltonian, and $t' = 0.68$ eV, which gives a much better approximation to real graphene [39], although other parametrizations with a lower value of t' are available [40]. Here we analyze the worst case scenario, i.e., a large value for t'. As we will see, our results are robust for such a large value. The idea is to study the effects of including next-to-nearest neighbor hopping interaction in the problem of localization. The third sum is over impurity sites with self-energy ε. The number of impurities sites, N_{imp}, is determined by the concentration $C = N_{\text{imp}}/N_{\text{T}}$, where N_{T} is the total number of sites on the honeycomb lattice.

Close to the Dirac energy $E = E_{\text{D}} = 0$, the model described by equation (1) presents exponentially localized wavefunctions, as has been documented in a previous publication by our group [26], and can even support strictly confined states [27] at $E = E_{\text{D}}$. Such wavefunctions are in agreement with the Abrahams *et al* theorem [15]. Here, we will concentrate on wavefunctions that are above the pseudomobility edge, which has been proven to have a size given by $\Delta \approx t\sqrt{6C}$ [7, 26].

In figure 1 we present a sample of the observed wavefunctions $\psi\left(\boldsymbol{r}\right)$ which solve the Schrödinger equation $H\psi\left(\boldsymbol{r}\right) = E\psi\left(\boldsymbol{r}\right)$ for an energy close to the Dirac energy, E_{D}, but outside the region where the participation ratio begins to decrease [7]. As can be seen, there is a progressive change of the localization as C or ε increases. However, although disorder increases up to a concentration of $C = 0.1$, no evident localization center appears. This suggests that one should perform a multifractal analysis to confirm this hypothesis. To do this, we will select some representative states, as shown in figure 2 on top of the density of states (DOS) for pure and doped graphene, considering $t' = 0$ and $t' \neq 0$.

The multifractal analysis can be performed as follows [41]. The system with area $A = N \times N$, where N is a number of primitive cells per side[2], is divided into $B = N^2/L^2$ boxes of linear size L. On a given box b, the probability of finding the electron is given by

$$\mu_b\left(\psi, L\right) = \sum_{\boldsymbol{r}\,\in\text{box }b}\left|\psi\left(\boldsymbol{r}\right)\right|^2. \tag{2}$$

A measure is built by normalizing the moments of this probability,

$$\mu_b\left(q, \psi, L\right) = \frac{\left[\mu_b\left(\psi, L\right)\right]^q}{P\left(q, \psi, L\right)}, \tag{3}$$

[2] Then, the number of total sites in the sample is $N_{\text{T}} = 2N^2$.

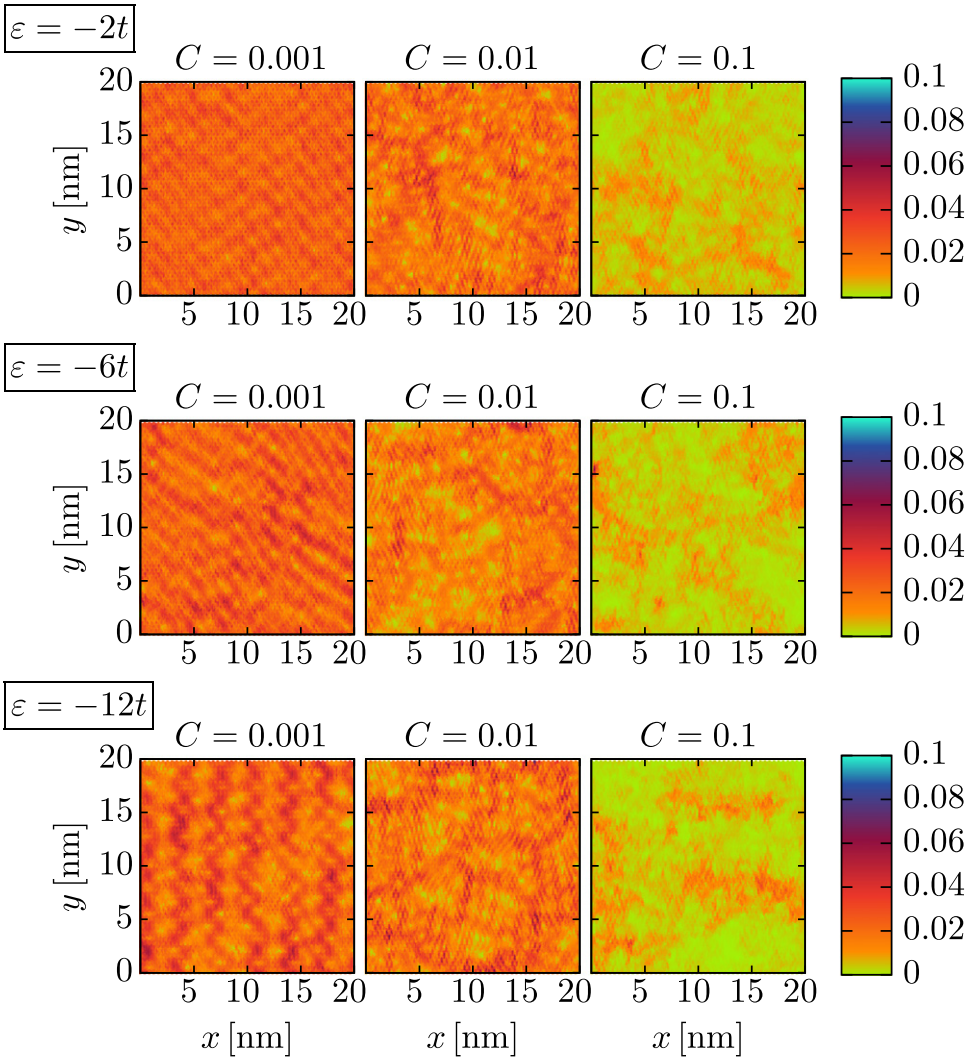

Figure 1. Electron wavefunction amplitude close to the Dirac point, but outside the region where the participation ratio begins to decrease, corresponding to $E = E_{\mathrm{D}} - 0.6t$, for different concentrations of disorder ($C = 0.001$, $C = 0.01$ and $C = 0.1$) and different impurity self-energ ($\varepsilon = -2t$, $\varepsilon = -6t$ and $\varepsilon = -12t$), using a lattice of $N_{\mathrm{T}} = 18\,432$ sites.

where $P\left(q, \psi, L\right)$ is,

$$P\left(q, \psi, L\right) = \sum_{b=1}^{B} \left[\mu_b\left(q, \psi, L\right)\right]^q. \tag{4}$$

The mass exponent of the wave function can be obtained using

$$\tau_q\left(\psi\right) = \lim_{\delta \to 0} \frac{P\left(q, \psi, L\right)}{\ln \delta}, \tag{5}$$

where δ is the ratio L/N. The fractal dimensions D_q is introduced via [29] $D_q = \tau_q/\left(q - 1\right)$. In an insulator $D_q = 0$ while for a metal $D_q = d$. In multifractal cases, D_q is a function of q.

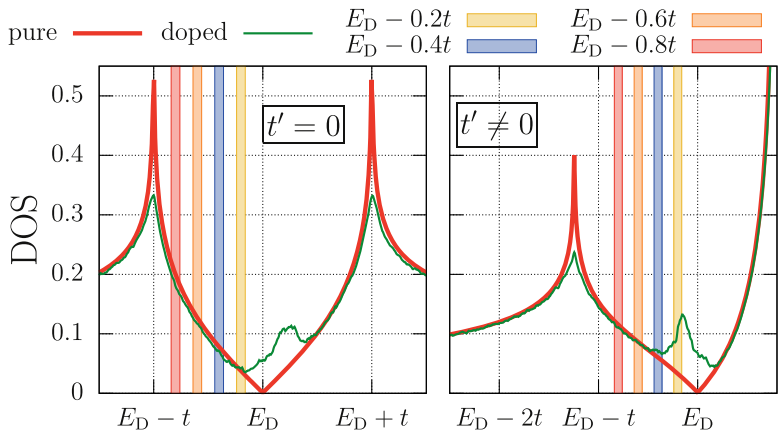

Figure 2. Density of states (DOS) for pure and doped graphene. The color bands indicate the energies used to study $f\left(\alpha\right)$. The left panel corresponds to the case $t' = 0$ while the other to $t' \neq 0$. In both graphs, the parameters are $N_T = 28\,800$, $C = 0.05$ and $\varepsilon = -6t$.

Using the previous equation (3), it is possible to find the singularity spectrum $f\left(\alpha_q\right)$, which is basically the fractal dimension of the set of points where the wavefunction behaves as $\left|\psi\left(\boldsymbol{r}\right)\right|^2 \sim L^{-\alpha_q}$ [42]. For a finite system, the number of such points scales as $L^{f\left(\alpha_q\right)}$. This singularity spectrum $f\left(\alpha_q\right)$ is obtained by observing that,

$$\alpha_q\left(\psi\right) = \lim_{\delta\to 0}\frac{A\left(q,\psi,L\right)}{\ln\delta}, \tag{6}$$

where $A\left(q,\psi,L\right)$ is,

$$A\left(q,\psi,L\right) = \left\langle \sum_{b=1}^{B}\mu_b\left(q,\psi,L\right)\ln\mu_b\left(1,\psi,L\right)\right\rangle. \tag{7}$$

Here $\langle\ldots\rangle$ denotes the arithmetic average over many realizations of disorder. In figure 3, the typical behavior of $A\left(q,\psi,L\right)$ is plotted as a function of δ for several q. For each q, a straight line can be fitted in order to obtain the slope and from there obtain α_q. The singularity spectrum $f\left(\alpha_q\right)$ is obtained as,

$$f\left(\alpha_q\right) = \lim_{\delta\to 0}\frac{F\left(q,\psi,L\right)}{\ln\delta}, \tag{8}$$

where $F\left(q,\psi,L\right)$ is a kind of entropy information,

$$F\left(q,\psi,L\right) = \left\langle \sum_{b=1}^{B}\mu_b\left(q,\psi,L\right)\ln\mu_b\left(q,\psi,L\right)\right\rangle, \tag{9}$$

where $F\left(q,\psi,L\right)$ can be calculated as done with $A\left(q,\psi,L\right)$, since all points fall in a straight line as a function of δ (figure 3).

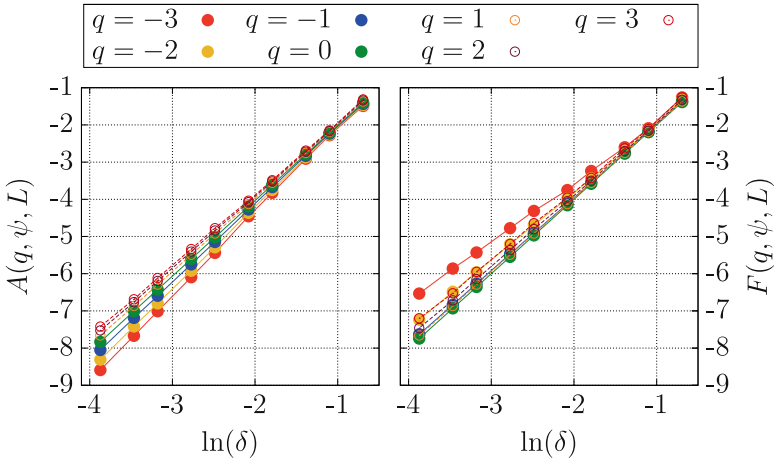

Figure 3. Left panel: typical behavior of $A\left(q, \psi, L\right)$. Right panel: typical behavior of $F\left(q, \psi, L\right)$. In both graphs, the parameters are $E = E_{\mathrm{D}} - 0.2t$, $\varepsilon = -6t$ and $C = 0.0001$.

As a control of the involved analysis, we have verified that for pure graphene $\varepsilon = 0$, the singularity spectrum converges to the point $f\left(2\right) = 2$, which is exactly the expected value for Bloch states in 2 dimensions. In figure 4 we present the singularity spectrum for three states at $E = E_{\mathrm{D}} - 0.2t$, $E_{\mathrm{D}} - 0.6t$, $E_{\mathrm{D}} - 0.8t$, chosen to represent states near and far from the Dirac energy. The criterion used to define such energies was in proximity with the energy for the appereance of frustration, determined from a variational procedure [7] and given by $\Delta = t\sqrt{6C}$. For example, for values around $C = 0.01$, $\Delta \approx 0.25t$. At Δ, the inverse participation ratio presents a well documented increase [7]. Notice that it is possible to analyze states closer to zero than the one studied here and even at $E = 0$, however, such states are localized and strictly localized [27].

Figure 4 was made considering $\varepsilon = -6t$ for an average of 30 lattices of $N_{\mathrm{T}} = 28\,000$ sites, which correponds to a size 20 nm. The behavior with the system size of $f\left(\alpha\right)$ is presented in figure 6. It will be discussed after analyzing some properties of $f\left(\alpha\right)$.

First of all, a convex parabola is observed in figure 4, showing a typical weak multifractal behavior. This proves that multifractal states are present, which was the main hypothesis of this work. We have verified that the multifractal behavior is observed for many other states, as well as for a different set of disorder parameters C and ε (see below). Also, the figure shows the tendency for states near the Dirac point to have a wider multifractal distribution, while states far from E_{D} tend to have a more pronounced mono-fractal character, as expected from a frustration analysis of the underlying triangular symmetry of the lattice [9]. In fact, it is interesting to compare with the 2D limit of a strongly disordered system, in which exponentially localized states are observed with a spectrum that converges to the points $f\left(0\right) = 0$ and $f\left(\infty\right) = 2$. This tendency for states near the Dirac point was also confirmed in this work as disorder was increased, since the parabola $f\left(\alpha\right)$ tends to reach the origin, and at the same time spreads over bigger values of α, indicating a tendency for localization. Such spreading can be quantified

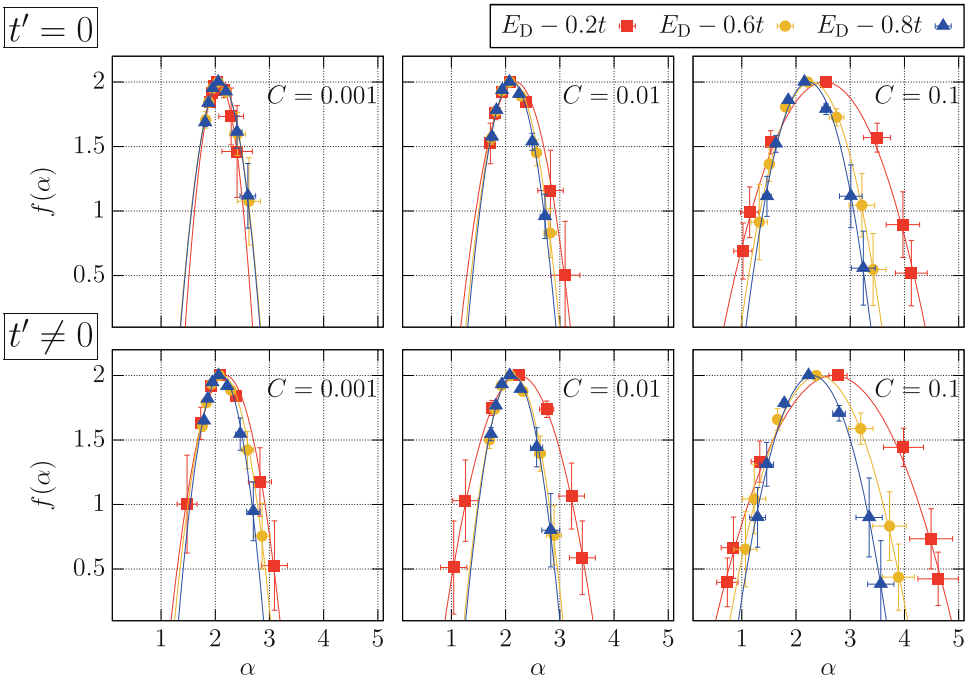

Figure 4. Singularity spectrum for three representative states. A state near the Dirac energy $E_D - 0.2t$ (red squares), $E_D - 0.4t$ (gold circles), and far from E_D at $E_D - 0.8t$ (blue triangles). Here $\varepsilon = -6t$. The first row corresponds to the nearest-neighbor interaction $t' = 0$, while the second corresponds to the next-to-nearest neighbor hopping interaction $t' \neq 0$. The solid lines were obtained by fitting the data with a parabola. Notice how the state far from the Dirac point always has a more pure fractal behavior than its counterparts. The plot was made using an average over 30 lattices of $N_T = 18\,432$ sites.

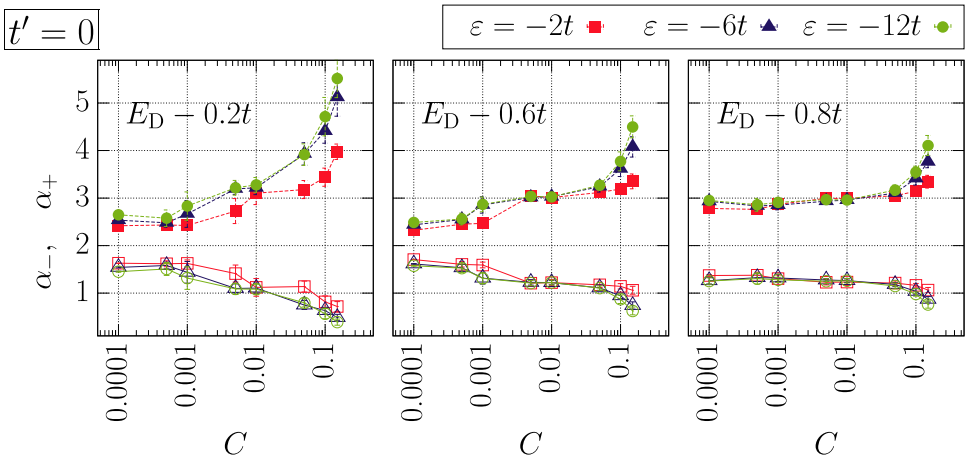

Figure 5. Evolution of the roots of $f(\alpha)$ (α_- open symbols and α_+ filled symbols) as a function of the impurity concentration for the states at $E = E_D - 0.2t$, $E_D - 0.6t$, $E_D - 0.8t$, using different values of ε for nearest-neighbor hopping.

by looking at the roots of $f(\alpha)$, denoted by α_- and α_+ with $\alpha_- < \alpha_+$; as shown in figure 5. In this figure, one can observe how for small disorder, the roots tend to merge, as expected for states which are closer to a Bloch behavior. The spreading becomes bigger for high C and ε. Another important feature is the value α_0 for which $f(\alpha_0) = 2$, corresponding to the maximal value of $f(\alpha)$. Due to this property, in the limit $N \to \infty$, for almost all points the amplitudes scale as $|\psi(\boldsymbol{r})|^2 \sim L^{-\alpha_0}$, where $\alpha_0 > 2$. This confirms that eigenfunctions follow a power law decay, a point that was already discussed in great detail in a previous publication [26].

For real graphene, the next-to-nearest neighbor hopping interaction is important. In figure 4 we present $f(\alpha)$ for the same three states and parameters including t'. Notice how states close to the Dirac point are more localized, while the state far from the Dirac point is nearly equal to its counterpart in figure 4. The appearance of this more pronounced behavior is still an open question since $t' \neq 0$ breaks the bipartite nature of the network.

Taking into account the debate on metal-insulator transitions in 2D [16], an important issue concerning our observations is how the results are scaled with the system size. Although such detailed analysis has been done before for the generalized inverse participation ratio [26], in figure 6 we present the scaling of $f(\alpha)$ as a function of the system size. It is possible to see how multifractal states far from the Dirac energy show a good convergence. Excluding the state close to the Fermi energy at $E = E_D - 0.2t$, all others show a tendency to display an extended nature in this scale. This can be seen in figure 6 by observing that bigger sizes tend to sharpen the distribution and collapse the points close to the value for extended states. Localized states show the opposite behavior as has been explained previously, i.e., the spectrum converges to the points $f(0) = 0$ and $f(\infty) = 2$. Thus, the scaling of $f(\alpha)$ shows no evidence for localization for the system sizes considered here.

In figure 7, the evolution of D_q is presented for the same three states using $\varepsilon = -6t$ at different C. The reduced dispersion of D_q for $E = E_D - 0.8t$ again indicates a less dispersed mono-fractal character of states far from E_D. An interesting quantity to look for is the anomalous dimension Δ_q defined as,

$$\Delta_q \equiv \tau_q - 2(q-1), \tag{10}$$

which separates the normal part in such a way that distinguishs the metallic phase from the critical point and determines the scale dependence of the wave function correlations. In figure 8 we present the corresponding result for Δ_q using the same set of parameters used in previous equations. The most important feature to remark in the plot is the absence of symmetry around $q = 0$. As we will see below, this allows one to discuss the type of the broken symmetries when disorder is included. It is worth mentioning that the value Δ_2 gives the decaying exponent of the wave function amplitude correlations [43], i.e.,

$$N^4 \left\langle \left| \psi^2(\boldsymbol{r}) \psi^2(\boldsymbol{r}') \right| \right\rangle \sim \left(\frac{|\boldsymbol{r} - \boldsymbol{r}'|}{N} \right)^{-\eta}, \tag{11}$$

with $\Delta_2 = -\eta$. This confirms again that wave functions close to the Dirac point decay faster, since from figure 8, $|\Delta_2|$ is bigger than the corresponding values for states far from E_D.

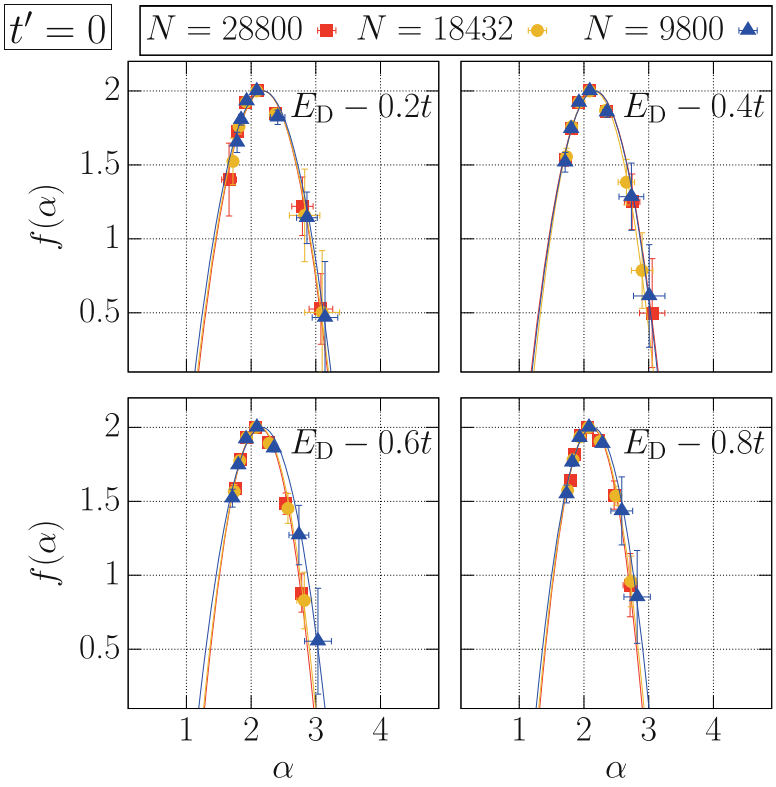

Figure 6. Singularity spectrum for three representative system sizes. A $N_T = 9800$ sample (blue triangles), $N_T = 18\,432$ sample (gold circles), and $N_T = 28\,800$ sample (red squares). In this panel $\varepsilon = -6t$ and $C = 0.01$. The top left panel corresponds to a state near the Dirac energy $E_D - 0.2t$, the top right panel to the energy $E_D - 0.4t$, the bottom left panel to a energy far from the Dirac energy $E_D - 0.6t$ and the bottom right panel to a energy near to the Van Hove singularity. The figure illustrates the slight dependence of the singularity spectrum as the sample size is increased, except for the energy near the E_D.

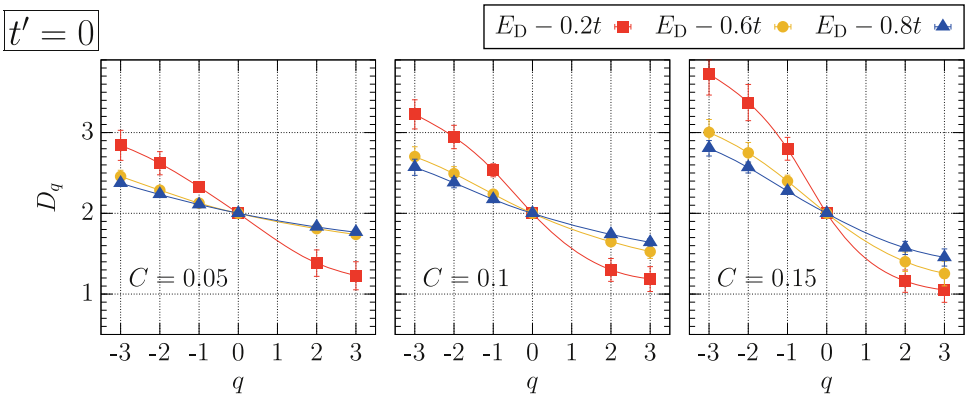

Figure 7. D_q as a function of q for three representative states using $\varepsilon = -6t$, obtained by averaging over 30 lattices of $N_T = 18\,432$ sites.

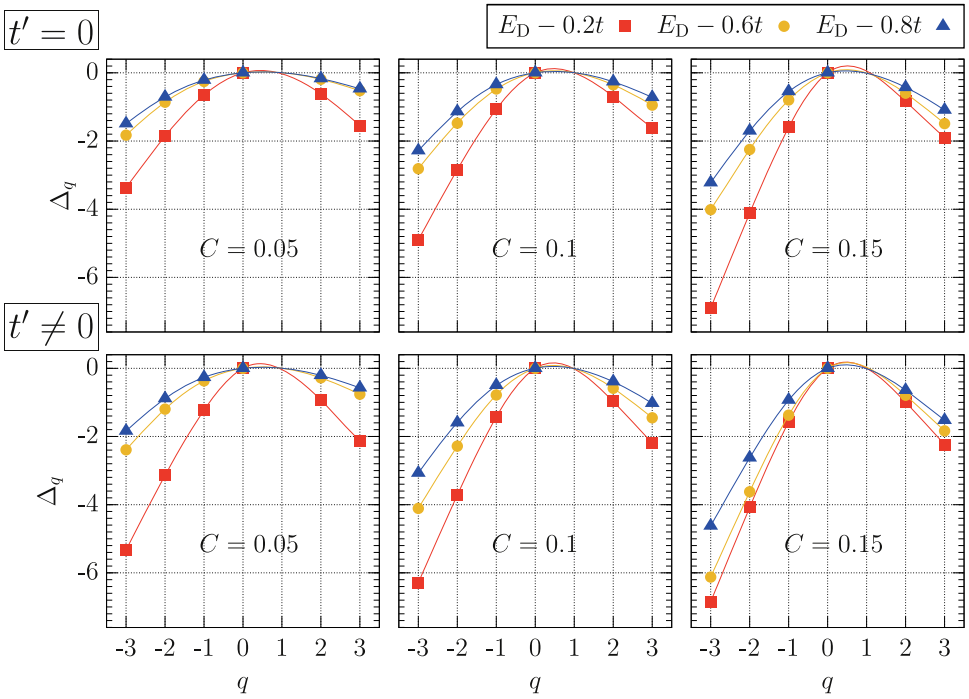

Figure 8. Δ_q for three different states using the same set of parameters of the previous plot. Notice the asymmetry with respect to $q = 0$. The top panel corresponds to the nearest-neighbor hopping interaction $t' = 0$ and bottom panel corresponds to the next-to-nearest neighbor hopping interaction $t' \neq 0$.

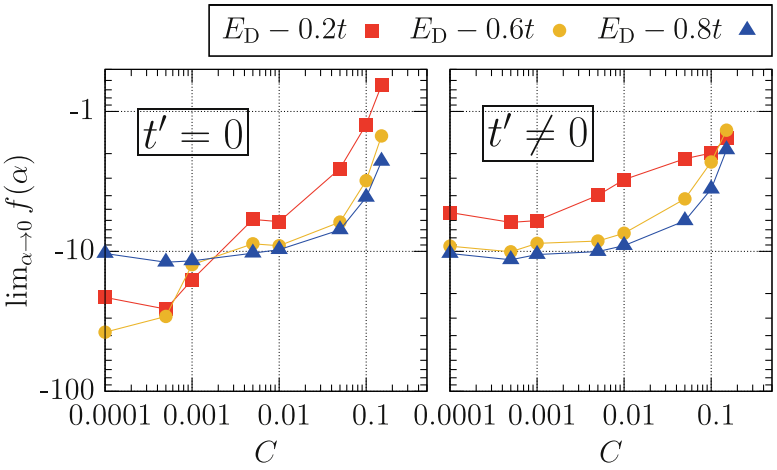

Figure 9. Values of $f(\alpha)$ at $\alpha = 0$ for different states as a function of C for $\varepsilon = -12t$.

One can extract more information on the nature of the singularity spectrum when disorder is included by calculating the behavior of $f(\alpha \to 0)$ as a function of the impurity concentration. Three kinds of behaviors are known [29], (a) no singularity when $\lim_{\alpha\to 0} f(\alpha) = -\infty$, (b) termination when $\lim_{\alpha\to 0} f(\alpha) =$ constant and (c) freezing when $\lim_{\alpha\to 0} f(\alpha) = 0$. In figure 9

we present the results obtained from our simulation, where $f\left(0\right)$ was obtained by looking at each $f\left(\alpha\right)$ fitting. From figure 9, the results indicate that all plots correspond to case b), with a tendency to reach freezing as the disorder increases.

According to the random matrix ensemble symmetry analysis in the context of graphene [44], multifractality arises due to a breaking of the Dirac Hamiltonian symmetries. Such a Hamiltonian contains a bipartite symmetry which is inherited from the fact that two atoms are present in the graphene's unitary cell. Each kind of perturbation leads to different broken symmetries. In the case of vacancies, which is akin to our *split band limit case* $\varepsilon/t \to \infty$, the chiral, temporal and isospin symmetries are preserved but are active only at the band center. The resulting Hamiltonian belongs to the chiral ortogonal symmetry (BDI class), resulting in a Gade–Wegner-type theory, characterized by lines of fixed points for the renormalization group and non-universal conductivity [29]. In this class, the localization transition corresponds to the case of termination for weak disorder and freezing for strong disorder, a tendency that seems to be confirmed by our plots of Δ_q (figure 8) and $f\left(\alpha = 0\right)$ (figure 9). However, the absence of symmetry in Δ_q with respect to q in figure 8 for finite ε/t seems to suggest that the results do not belong to the Wigner–Dyson class.

In fact, note that for finite ε/t, the disorder introduced by us does not correspond to the BDI class, since chirality is not preserved, basically because there are elements in the diagonal of the Hamiltonian matrix which leads to a non symmetric spectrum around the Dirac point, as shown in figure 2. Theoretically, the corresponding class is AI, which is inside the Wigner–Dyson class, for any finite value of the on-site energy. However, in the limit $\varepsilon \gg t$, the symmetry is reestablished in the carbon band [7, 45], leading to a chiral BDI symmetry. In other words, impurities with $\varepsilon \gg t$ can be also treated by setting all bonds connected to an impurity with a hopping parameter $t = 0$. Thus, our model reduces to the analysis made by Ostrovsky *et al* [44] in the case $\varepsilon \gg t$, where the orthogonal symmetry class implies strong localization.

Thus, since the theoretical model for finite ε/t implies a Wigner–Dyson class with a symmetrical Δ_q, while our numerical results suggest a non-symmetrical one, several scenarios are possible. Either the observed universality class is not embedded in the class of the Hamiltonian, leading to a very slow renormalization group flow not seen by the small sizes treated here, or statistical fluctuations are too strong. In future work we will discuss this issue, which is beyond the scope of this letter.

Finally, it is worth mentioning that the model given by equation (1) for a binary distribution of self-energies in the split-band limit $\varepsilon \gg t$ reduces to the problem of quantum site percolation in a hexagonal lattice. Thus, our results can be extended in a natural way to the same problem.

In conclusion, we have given numerical evidence of the multifractal nature of wave functions in doped graphene for system sizes smaller than the possible localization length. This is important to understand the conductance of small system sizes, since according to our results, it will depend on the system length. Such an effect can appear in graphene with H adatoms [6] or doped nanoribbons. Also, this effect can be tested in doped polycrystalline graphene [46] with sizes lower than 20 nm.

Acknowledgments

This work was supported by DGAPA-UNAM project under grant IN-102513. Computations were done at supercomputer NES of DGTIC-UNAM.

References

[1] Novoselov K S, Geim A K, Morozov S V, Jiang D, Zhang Y, Dubonos S V, Grigorieva I V and Firsov A A 2004 *Science* **306** 666–9
[2] Novoselov K S, Jiang D, Schedin F, Booth T J, Khotkevich V V, Morozov S V and Geim A K 2005 *Proc. Natl Acad. Sci. USA* **102** 10451–3
[3] Geim A K and Novoselov K S 2007 *Nat. Mater.* **6** 183–91
[4] Balandin A A, Ghosh S, Bao W, Calizo I, Teweldebrhan D, Miao F and Lau C N 2008 *Nano Lett.* **8** 902–7
[5] Geim A K 2009 *Science* **324** 1530–4
[6] Bostwick A, McChesney J L, Emtsev K V, Seyller T, Horn K, Kevan S D and Rotenberg E 2009 *Phys. Rev. Lett.* **103** 056404
[7] Naumis G G 2007 *Phys. Rev.* B **76** 153403
[8] Martinazzo R, Casolo S and Tantardini G F 2010 *Phys. Rev.* B **81** 245420
[9] Barrios-Vargas J E and Naumis G G 2011 *J. Phys.: Condens. Matter* **23** 375501
[10] Katoch J, Chen J H, Tsuchikawa R, Smith C W, Mucciolo E R and Ishigami M 2010 *Phys. Rev.* B **82** 081417
[11] Peres N M R 2010 *Rev. Mod. Phys.* **82** 2673–700
[12] Robinson J P, Schomerus H, Oroszlány L and Fal'ko V I 2008 *Phys. Rev. Lett.* **101** 196803
[13] la Magna A, Deretzis I, Forte G and Pucci R 2009 *Phys. Rev.* B **80** 195413
[14] Deretzis I, Fiori G, Iannaccone G and la Magna A 2010 *Phys. Rev.* B **81** 085427
[15] Abrahams E, Anderson P W, Licciardello D C and Ramakrishnan T V 1979 *Phys. Rev. Lett.* **42** 673–6
[16] Schubert G and Fehske H 2008 *Phys. Rev.* B **77** 245130
[17] Bunde A, Kantelhardt J W and Schweitzer L 1998 *Ann. Phys., Lpz.* **7** 372–82
[18] Haldas G, Kolek A and Stadler A 2002 *Phys. Status Solidi b* **230** 249–52
[19] Eilmes A, Römer R A and Schreiber M 2001 *Physica B Condens. Matter* **296** 46–51
[20] Nazareno H N, de Brito P E and Rodrigues E S 2002 *Phys. Rev.* B **66** 012205
[21] Schreiber M and Grussbach H 1992 *Phil. Mag.* B **65** 707–14
[22] Bardarson J H, Tworzydło J, Brouwer P W and Beenakker C W J 2007 *Phys. Rev. Lett.* **99** 106801
[23] Nomura K, Koshino M and Ryu S 2007 *Phys. Rev. Lett.* **99** 146806
[24] Pereira V M, Lopes dos Santos J M B and Castro Neto A H 2008 *Phys. Rev.* B **77** 115109
[25] Song Y, Song H and Feng S 2011 *J. Phys.: Condens. Matter* **23** 205501
[26] Barrios-Vargas J E and Naumis G G 2012 *J. Phys.: Condens. Matter* **24** 255305
[27] Barrios-Vargas J E and Naumis G G 2013 *Solid State Commun.* **162** 23–27
[28] Lee K L, Grémaud B, Miniatura C and Delande D 2013 *Phys. Rev.* B **87** 144202
[29] Evers F and Mirlin A D 2008 *Rev. Mod. Phys.* **80** 1355–417
[30] González J, Guinea F and Vozmediano M A H 2001 *Phys. Rev.* B **63** 134421
[31] Amanatidis I and Evangelou S N 2009 *Phys. Rev.* B **79** 205420
[32] Amanatidis E, Kleftogiannis I, Katsanos D E and Evangelou S N 2014 *J. Phys.: Condens. Matter* **26** 155601
[33] Srivastava V and Weaire D 1978 *Phys. Rev.* B **18** 6635–8
[34] Meir Y, Aharony A and Harris A B 1989 *Europhys. Lett.* **10** 275
[35] Soukoulis C M and Grest G S 1991 *Phys. Rev.* B **44** 4685–8
[36] Schweitzer L and Markos P 2008 *Phys. Rev.* B **78** 205419
[37] Markoš P and Schweitzer L 2012 *Physica: B Condens. Matter* **407** 4016–22

[38] Wallace P R 1947 *Phys. Rev.* **71** 622–34
[39] Reich S, Maultzsch J, Thomsen C and Ordejón P 2002 *Phys. Rev.* B **66** 035412
[40] Nanda B R K and Satpathy S 2009 *Phys. Rev.* B **80** 165430
[41] Thiem S and Schreiber M 2013 *Eur. Phys. J.* B **86** 1–10
[42] Halsey T C, Jensen M H, Kadanoff L P, Procaccia I and Shraiman B I 1986 *Phys. Rev.* A **33** 1141–51
[43] Abrahams E 2010 *50 Years of Anderson Localization* (Singapore: World Scientific)
[44] Ostrovsky P M, Gornyi I V and Mirlin A D 2007 *Eur. Phys. J. Spec. Top.* **148** 63–72
[45] Barrios-Vargas J E and Naumis G G 2011 *Phil. Mag.* **91** 3844–57
[46] van Tuan D, Kotakoski J, Louvet T, Ortmann F, Meyer J C and Roche S 2013 *Nano Lett.* **13** 1730–5